IJMMM International Journal of Minerals, Metallurgy and Materials 矿物冶金与材料学报（英文版）

Effect of solvents on the morphology and structure of barium titanate synthesized by a one-step hydrothermal method

Xiaoxiao Pang, Tingting Wang, Bin Liu, Xiayue Fan, Xiaorui Liu, Jing Shen, Cheng Zhong, and Wenbin Hu

Cite this article as:
Xiaoxiao Pang, Tingting Wang, Bin Liu, Xiayue Fan, Xiaorui Liu, Jing Shen, Cheng Zhong, and Wenbin Hu, Effect of solvents on the morphology and structure of barium titanate synthesized by a one-step hydrothermal method, *Int. J. Miner. Metall. Mater.*, 30(2023), No. 7, pp. 1407-1416. https://doi.org/10.1007/s12613-023-2614-9

View the article online at SpringerLink or IJMMM Webpage.

International Journal of Minerals, Metallurgy and Materials
Volume 30, Number 7, July 2023, Page 1407
https://doi.org/10.1007/s12613-023-2614-9

Effect of solvents on the morphology and structure of barium titanate synthesized by a one-step hydrothermal method

Xiaoxiao Pang[1)], *Tingting Wang*[1)], *Bin Liu*[1)], *Xiayue Fan*[1)], *Xiaorui Liu*[1)], *Jing Shen*[2)], *Cheng Zhong*[1,3),✉], *and Wenbin Hu*[1,3)]

1) Key Laboratory of Advanced Ceramics and Machining Technology (Ministry of Education), and Tianjin Key Laboratory of Composite and Functional Materials, School of Materials Science and Engineering, Tianjin University, Tianjin 300072, China
2) Chongqing Newcent New Materials Co., Ltd., Chongqing 401147, China
3) Joint School of National University of Singapore and Tianjin University, International Campus of Tianjin University, Fuzhou 350207, China
(Received: 14 September 2022; revised: 13 February 2023; accepted: 17 February 2023)

Abstract: Tetragonal barium titanate was synthesized from barium hydroxide octahydrate and titanium tetrachloride through a simple one-step hydrothermal method. The effect of different solvents on the crystal structure and morphology of barium titanate nanoparticles during the hydrothermal process was investigated. Except for ethylene glycol/water solvent, impurity-free barium titanate was synthesized in pure water, methanol/water, ethanol/water, and isopropyl alcohol/water mixed solvents. Compared with other alcohols, ethanol promotes the formation of a tetragonal structure. In addition, characterization studies confirm that particles synthesized in methanol/water, ethanol/water, and isopropyl alcohol/water mixed solvents are smaller in size than those synthesized in pure water. In the case of alcohol-containing solvents, the particle size decreases in the order of isopropanol, ethanol, and methanol. Among all the media used in this study, ethanol/water is considered the optimum reaction media for barium titanate with high tetragonality (defined as the ratio of two lattice parameters c and a, c/a = 1.0088) and small average particle size (82 nm), which indicates its great application potential in multilayer ceramic capacitors.

Keywords: barium titanate; hydrothermal synthesis; tetragonality; solvent effects

1. Introduction

Barium titanate ($BaTiO_3$) has a broad application potential in the dielectric ceramics industry, particularly multilayer ceramic capacitors (MLCCs), because of its outstanding dielectric, ferroelectric, piezoelectric, and pyroelectric performances [1–2]. Among the numerous structures of $BaTiO_3$, the tetragonal structure is prominent, in which the Ti^{4+} cation deviates from the center of [TiO_6] octahedron, and the displacement of the cation center deviates from the center of the anion, resulting in net polarization along the [001] edge direction. Therefore, tetragonal $BaTiO_3$ exhibits ferroelectricity with spontaneous polarization following the orientation of the c-axis, which directly affects the dielectric constant of $BaTiO_3$ ceramics [3–5]. A significant property of tetragonal $BaTiO_3$ is the extent of tetragonal distortion of the cell structure, which is known as tetragonality (c/a), defined as the ratio of two lattice parameters c and a [6]. Tetragonality is a commonly used index to describe the ferroelectricity of tetragonal $BaTiO_3$ [7–8] and determines the dielectric properties of $BaTiO_3$ using a positive correlation [9]. Therefore, $BaTiO_3$ with high tetragonality is desired for obtaining good ferroelectric and dielectric properties, which promotes the application of $BaTiO_3$ in MLCCs [10].

Recently, the demand for MLCCs with thin dielectric layers and ultra-high capacity has increased considerably as electronic devices move toward miniaturization and multifunctionality. As the layer thickness of the dielectric further decreases to 0.5 μm, the dimension of $BaTiO_3$ powders needs to be controlled within 100 nm [11]. Therefore, the particle size in $BaTiO_3$ powders generally shows a decreasing trend.

However, $BaTiO_3$ nanoparticles have a size effect, where the tetragonality of $BaTiO_3$ nanoparticles decreases with the decrease of the particle size [12]. Preparing $BaTiO_3$ nanoparticles with high tetragonality and small particle size is difficult. Thus, various efforts have been exerted to prepare $BaTiO_3$ with high tetragonality and tiny particle size. Tetragonal $BaTiO_3$ powders are traditionally prepared using the solid-state reaction of $BaCO_3$ and TiO_2 at a high temperature of above 900°C [13–14]. Nonetheless, the prepared $BaTiO_3$ powders cannot meet the increasing demand for the miniaturization of electronic devices because of their large size and uncontrolled morphology caused by high synthesis temperature [15–16]. In addressing these issues, many wet

✉ Corresponding author: Cheng Zhong E-mail: cheng.zhong@tju.edu.cn

chemical methods have been explored for $BaTiO_3$ nanoparticles. Among these methods, the hydrothermal process shows great application potential because of its uniform particle size and controllable morphology of $BaTiO_3$ nanoparticles [17]. Nevertheless, $BaTiO_3$ nanoparticles prepared by using a hydrothermal method usually have a cubic structure or tetragonal structure with low tetragonality [18]. Peng *et al.* [19] used barium hydroxide and tetrabutyl titanate as precursors to prepare $BaTiO_3$ nanoparticles at 200°C for 48 h. The obtained nanoparticles were nearly spherical and highly dispersed, with a particle size of 70–80 nm. But $BaTiO_3$ primarily possessed a cubic phase with a small amount of tetragonal phase. Hayashi and Ebina [20] hydrothermally synthesized $BaTiO_3$ particles using TiO_2 sol and $Ba(OH)_2$ as reactants at 250–400°C. The data of c/a = 1 showed that $BaTiO_3$ synthesized at 250–350°C exhibited a cubic phase. The tetragonality of $BaTiO_3$ synthesized at 400°C was 1.007. In order to transform a cubic into a tetragonal structure or enhance the tetragonality, the hydrothermal duration or calcination at a high temperature is increased [21–22]. Huang *et al.* [23] synthesized $BaTiO_3$ powders with high tetragonality up to 1.0094 by a two-step hydrothermal method. Hasbullah *et al.* [24] calcined the powders at a high temperature of 500–1000°C for 4 h after the hydrothermal process at 200°C for 72 h. $BaTiO_3$ calcined at 700°C and 1000°C exhibited a tetragonal structure with tetragonality of 1.0022 and 1.0100, respectively. However, barium carbonate impurity was introduced during calcination, which affected the purity of $BaTiO_3$. Therefore, the preparation of $BaTiO_3$ nanoparticles with a small size, uniform morphology, and high tetragonality by using a one-step hydrothermal method remains a challenging task. In addition, the factors affecting the hydrothermal synthesis of tetragonal $BaTiO_3$ nanoparticles are complex. Among them, the nature of reaction media significantly affects the solubility of reactants as well as the nucleation and growth of crystals [25]. Mo *et al.* [26] reported the hydrothermal preparation of $BaTiO_3$ powder using isopropanol and ethanol as additives. The particle size was controlled by adjusting the volume fraction of alcohol or isopropanol. Nakashima *et al.* [27] investigated the surface reconstruction of $BaTiO_3$ nanocubes. The result showed that the morphology of $BaTiO_3$ was dependent on the reaction medium. However, the influence of solvent types on the crystal structure and morphology of $BaTiO_3$ nanoparticles prepared by using a hydrothermal method has still received limited attention to date.

In this work, tetragonal $BaTiO_3$ nanoparticles were synthesized through a simple, one-step hydrothermal method. The synthesis specifically used barium hydroxide octahydrate and titanium tetrachloride as raw materials and different solvents as the reaction medium at 240°C. The influence of different solvents on the crystal structure and morphology of $BaTiO_3$ nanoparticles synthesized by using a hydrothermal process was studied through X-ray diffraction (XRD), Raman spectroscopy, scanning electron microscopy (SEM), and transmission electron microscopy (TEM).

2. Experimental

2.1. Materials

Titanium tetrachloride ($TiCl_4$, 99.0%), barium hydroxide octahydrate ($Ba(OH)_2{\cdot}8H_2O$, 98%), ammonia solution (NH_4OH, 25%–28% NH_3 in H_2O), methanol (≥99.5%), and acetate (99.5%) were purchased from Shanghai Aladdin Biochemical Technology Co., Ltd, China. Ethanol (≥99.7%) and isopropyl alcohol (≥99.7%) were bought from Tianjin Yuanli Chemical Co., Ltd, China. Ethylene glycol (98%) was produced by Shanghai Macklin Biochemical Co., Ltd, China. All reagents were directly used after purchase.

2.2. Preparation of $BaTiO_3$ nanoparticles

$BaTiO_3$ nanoparticles were prepared using $TiCl_4$ and $Ba(OH)_2{\cdot}8H_2O$ through a one-step hydrothermal method. During preparation, 25 mmol of $TiCl_4$ and 5 mL of deionized water were thoroughly mixed. Then, 20 mL of NH_4OH was added under vigorous stirring to fully hydrolyze the $TiCl_4$ solution. The solution was centrifuged to obtain a precipitate. Afterward, the precipitate was evenly mixed with a mixed solution of 20 mL of alcohol and 5 mL of deionized water. In studying the influence of different solvents, equal volumes of alcohol/water mixed solvents and pure water were used as reaction media. Alcohols included methanol, ethanol, isopropyl alcohol, and ethylene glycol. In mixed solvents, the volume of different alcohols was kept constant. In addition, 37.5 mmol of $Ba(OH)_2{\cdot}8H_2O$ was dissolved in 15 mL of deionized water to prepare a barium hydroxide solution under heating and stirring in a water bath at 90°C. Barium hydroxide solution and titanium solution were then mixed in which the Ba/Ti molar ratio was 1.5:1. Excess barium was used to compensate for the small number of barium ions consumed by the formation of barium carbonate precipitate in the hydrothermal process. 10 mL of NH_4OH solution was mixed into the above solution to maintain the alkaline environment. The pH value of the above solution was measured and reached 13. The mixture was transferred to a 50 mL parapolyphenylene container, which was then placed into a stainless-steel autoclave. The sealed autoclave was heated at 240°C for 30 h and naturally cooled to room temperature. The obtained product was washed several times with acetate solution and deionized water to remove BaO or $BaCO_3$ or both and residue containing Cl^-, NH_4^+, and excess Ba^{2+}. $BaTiO_3$ powders were acquired after being dried at 80°C for 12 h and ground. $BaTiO_3$ nanoparticles prepared using pure water, methanol/water, ethanol/water, isopropyl alcohol/water and ethylene glycol/water as the reaction medium were coded as PW–BT, MeOH/W–BT, EtOH/W–BT, IPA/W–BT, and EG/W–BT, respectively.

2.3. Characterization of $BaTiO_3$ nanoparticles

The crystal phase characteristics of $BaTiO_3$ nanoparticles were characterized by XRD (D8 Advanced, Bruker Corp,

Germany) with Cu K_α radiation working at 40 kV and 40 mA at room temperature.

The local crystal structure of $BaTiO_3$ nanoparticles was further analyzed by Raman spectroscopy (Horiba LabRAM HR Evolution, Japan) with a 532 nm laser at room temperature. The measured Raman shift was in the range of 100–1200 cm^{-1}.

The morphology and particle size distribution of $BaTiO_3$ nanoparticles were researched by SEM (Hitachi S–4800, Japan). The average particle size and size distribution of $BaTiO_3$ nanoparticles were calculated by measuring the particle size of one hundred particles to reach sufficient statistics. The microstructure of $BaTiO_3$ nanoparticles was investigated by TEM (JEM–2100F, Japan).

The specific surface area and the distribution of pore size were measured through the N_2 sorption and desorption test using the Quantachrome QuadraSorb Station. The equivalent diameter (d_{BET}, nm) was determined by the following formula [28]: $d_{BET} = 6\times10^3/(\rho\times SSA)$, where SSA represents the specific surface ($m^2\cdot g^{-1}$), and ρ denotes the standard density (6.08 $g\cdot cm^{-3}$).

3. Results and discussion

3.1. XRD analysis

XRD is an important characterization method, which can be used for phase analysis of materials, the calculation of grain size, the determination of lattice parameters, etc. Fig. 1 exhibits the XRD patterns of $BaTiO_3$ samples prepared in different solvents. Except for EG/W–BT, the diffraction peaks are located between space group *P4mm* (JCPDS, No. 81–2201) of the tetragonal $BaTiO_3$ without impure peaks (Fig. 1(a)). The splitting of the (002) and (200) diffraction peaks is observed. Accordingly, tetragonal exists stably in $BaTiO_3$ nanoparticles synthesized in pure water, methanol/water, ethanol/water and isopropyl alcohol/water media. Furthermore, there are no other impure peaks. This demonstrates that the hydrothermal reactions in these four reaction media are relatively thorough. The crystal grains are well developed and free of impurities. Partial diffraction peaks of the EG/W–BT sample are indexed to those of tetragonal $BaTiO_3$ with space group *P4mm* (JCPDS No. 81–2201). There are many impurity peaks in the pattern, which are indexed as $Ba_2Ti_9O_{20}$, $BaTi_5O_{11}$, and unreacted TiO_2 in detail. This indicates that the hydrothermal reaction under the addition of ethylene glycol is not complete. The crystal grains are incompletely developed and accompanied by the formation of impurities. Compared with other solvents, ethylene glycol is not beneficial to the synthesis of tetragonal $BaTiO_3$ under this condition.

In order to analyze the tetragonal phase properties in detail, the enlarged parts of XRD spectra corresponding to the (002) and (200) planes of samples are provided to show distinct peak shifts from Fig. 1(b). The diffraction peaks around $2\theta = 45°$ have different degrees of splitting, which is evidence of the existence of the tetragonal structure. The peak with lower intensity appears at the smaller 2θ angle, corresponding to the (002) plane of the tetragonal $BaTiO_3$. The (200) peak with stronger intensity is located at the larger 2θ angle. The characteristic tetragonal peak of the MeOH/W–BT sample around $2\theta = 45°$ tends to split, but not obviously. The peaks converge into a single blunt peak, illustrating that the tetragonal features are not significant. The diffraction peaks of PW–BT and IPA/W–BT samples around

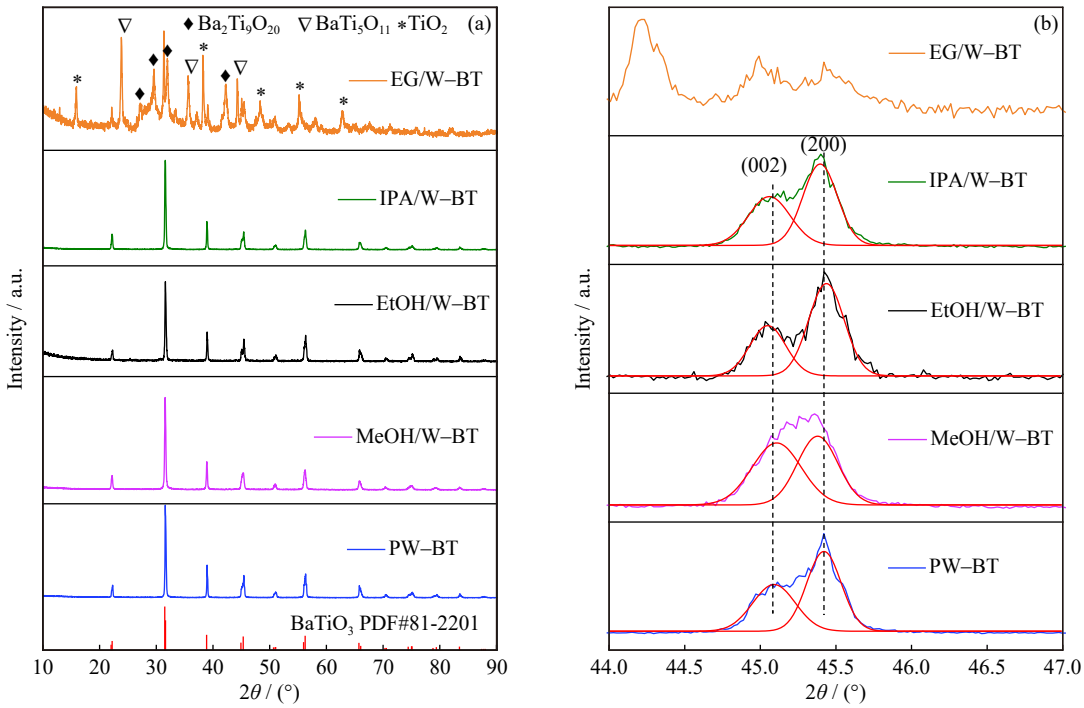

Fig. 1. (a) XRD patterns of $BaTiO_3$ samples prepared in different solvents. (b) Partially enlarged image of XRD patterns around $2\theta = 45°$. The solid red lines in (b) are Gaussian fitting lines of (002) and (200) peaks, respectively.

$2\theta = 45°$ display a trapezoidal splitting trend. By contrast, the diffraction peaks of the EtOH/W–BT sample around $2\theta = 45°$ are split into distinct doublets. This illustrates that the EtOH/W–BT sample possesses the most remarkable tetragonal characteristics, while the MeOH/W–BT sample has the weakest.

The diffraction peaks around $2\theta = 45°$ are deconvoluted into two peaks using the Gaussian function to explore the information of peak positions for tetragonal $BaTiO_3$ samples without impurities. Compared with the PW–BT sample, the 2θ angles corresponding to the (002) and (200) peaks of the MeOH/W–BT sample move towards each other, while it is opposite for the EtOH/W–BT sample. The positions of the (002) and (200) peaks for IPA/W–BT shift slightly from those of the PW–BT sample. $\Delta 2\theta$ is used to evaluate the relative position of the two peaks, defined as the difference between the 2θ angles of (002) and (200) fitting peaks, which is shown in Table 1. There is a certain relationship between the proportion of the tetragonal structure and the value of $\Delta 2\theta$. With the increase in the tetragonal phase content, the value of $\Delta 2\theta$ increases [23,29]. For MeOH/W–BT, the smallest $\Delta 2\theta$ value manifests the least tetragonal content. On the contrary, the EtOH/W–BT sample has the largest $\Delta 2\theta$ value illustrating the highest content of the tetragonal phase.

Table 1. Peak information of the (002) and (200) planes of MeOH/W–BT, EtOH/W–BT, IPA/W–BT, and PW–BT samples

Sample	2θ angle of (002) peak / (°)	2θ angle of (200) peak / (°)	$\Delta 2\theta$ / (°)
PW–BT	45.09	45.42	0.33
MeOH/W–BT	45.11	45.38	0.27
EtOH/W–BT	45.05	45.44	0.39
IPA/W–BT	45.06	45.40	0.34

The specific value of lattice parameters c and a is used to define the tetragonal distortion extent of the structure cell to evaluate the tetragonality of $BaTiO_3$ samples [30]. The splitting of the (200) and (002) peaks indicates the asymmetric extension of the crystal along the c-axis, which corresponds to the change in lattice parameters [31]. The lattice parameters and tetragonality of $BaTiO_3$ samples without impurities are shown in Fig. 2. The tetragonality of $BaTiO_3$ synthesized in pure water media is higher than that synthesized in monohydric alcohol/water. Among them, the tetragonal values of PW–BT and EtOH/W–BT samples are not much different, which are 1.0090 and 1.0088, respectively. Moreover, the tetragonality does not vary linearly in the order of methanol, ethanol, and isopropanol in the case of alcohol-containing solvents. Under the condition of ethanol/water medium, the tetragonality reaches the highest value ($c/a = 1.0088$) except for PW–BT. The tetragonality decreased after the addition of isopropyl alcohol. The tetragonality of the samples is all smaller than the theoretical value ($c/a = 1.0110$) [32]. The inhibited tetragonality is caused by the presence of defects [33].

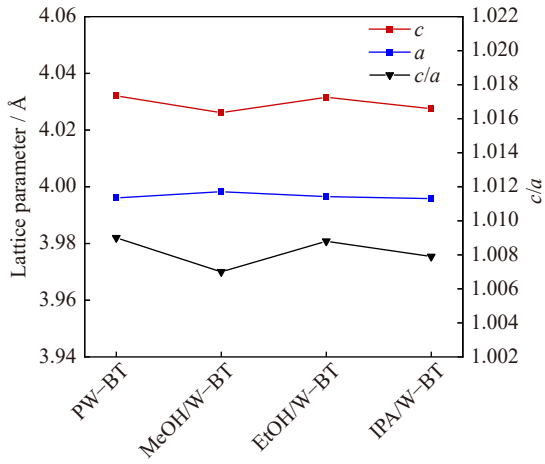

Fig. 2. Lattice parameters and tetragonality of MeOH/W–BT, EtOH/W–BT, IPA/W–BT, and PW–BT samples.

3.2. Raman spectra

Raman spectra were collected to detect the local lattice distortion of the $BaTiO_3$ nanoparticles. The Raman characteristic peaks of the $BaTiO_3$ tetragonal phase can be observed at 258, 306, 515, and 715 cm^{-1} for MeOH/W–BT, EtOH/W–BT, IPA/W–BT, and PW–BT samples, respectively (Fig. 3). The Raman peaks at 190, 258, and 515 cm^{-1} correspond to the fundamental transverse optical (TO) mode of the A_1 symmetry [3]. The band at 306 cm^{-1} is associated with the E(TO) or B_1 mode, indicating the asymmetry inside the $[TiO_6]$ octahedron of $BaTiO_3$ at the local scale [34]. The tetragonal phase prevails when the peaks at 306 cm^{-1} are clear and sharp. The wavelength band of 715 cm^{-1} is emitted by the longitudinal optical mode with the highest wave number of A_1 symmetry [35]. No other Raman bands attributable to impurities were found. Therefore, the Raman spectra reveal peaks belonging to tetragonal $BaTiO_3$ for MeOH/W–BT, EtOH/W–BT, IPA/W–BT, and PW–BT samples. Therefore, the tetragonal phase exists in MeOH/W–BT, although the characteristic peak of the tetragonal structure is a single peak in the XRD pattern (Fig. 1). The relative intensity of the peak at 306 cm^{-1} for PW–BT and EtOH/W–BT samples is higher and sharper than the others, indicating that the local tetragonal distortion is larger. Moreover, a correlation has been established between the characteristic peaks and the tetragonal

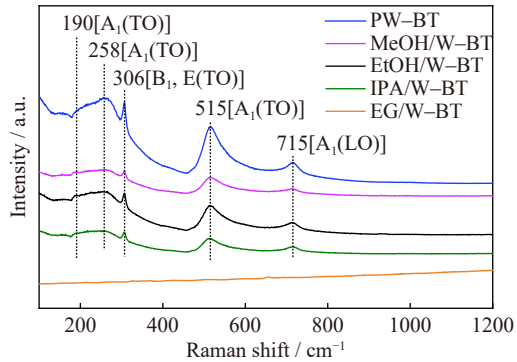

Fig. 3. Raman spectra of $BaTiO_3$ powders synthesized in different solvents.

characteristic [33]. The trend of peak intensity variation at 306 cm^{-1} is consistent with the tetragonality shown in Fig. 2. By contrast, the EG/W–BT sample has no evident Raman characteristic peaks. The sample has a fluorescence effect related to residual organic matter because of inadequate reaction after the addition of ethylene glycol into the solvent, which is commonly seen in Raman spectra [36].

3.3. SEM morphologies

The morphology and particle size of $BaTiO_3$ were analyzed by SEM. Fig. 4(a)–(e) shows SEM images of $BaTiO_3$ synthesized in different solvents. The $BaTiO_3$ sample obtained by using pure water as the solvent contains small spherical particles and irregular chunks (Fig. 4(a)). The aggregation of particles and chunks can be observed. After adding monohydric alcohols to the solvent, the samples are approximately spherical (Fig. 4(b)–(d)). Moreover, the particles are evenly distributed and well dispersed. Plate-like or rod-shaped particles are displayed in the SEM image of the EG/W–BT sample (Fig. 4(e)). Particles of different lengths are aggregated. Evidently, the solvent has a large influence on the morphology of $BaTiO_3$. The addition of monohydric alcohols increases the internal pressure in the closed space under a high-temperature environment, which promotes the hydrothermal reaction. The particles grow in an isotropic direction and form a spherical shape. In addition, monohydric alcohols play a role in dispersion, which reduces the aggregation of particles during growth [37]. When ethylene glycol is used as a solvent, the highest boiling point and viscosity lead to an insufficient hydrothermal reaction. The adhesion of ethylene glycol on particle surfaces of $BaTiO_3$ promotes the growth of particles in an anisotropic direction during the dissolution–precipitation process [38].

The particle size distribution of $BaTiO_3$ was collected (the inset in Fig. 4). A normal distribution plot is further drawn, which presents the distribution of particles about a certain size. The average particle sizes of samples synthesized in different solvents are shown in Fig. 4(f). The PW–BT sample

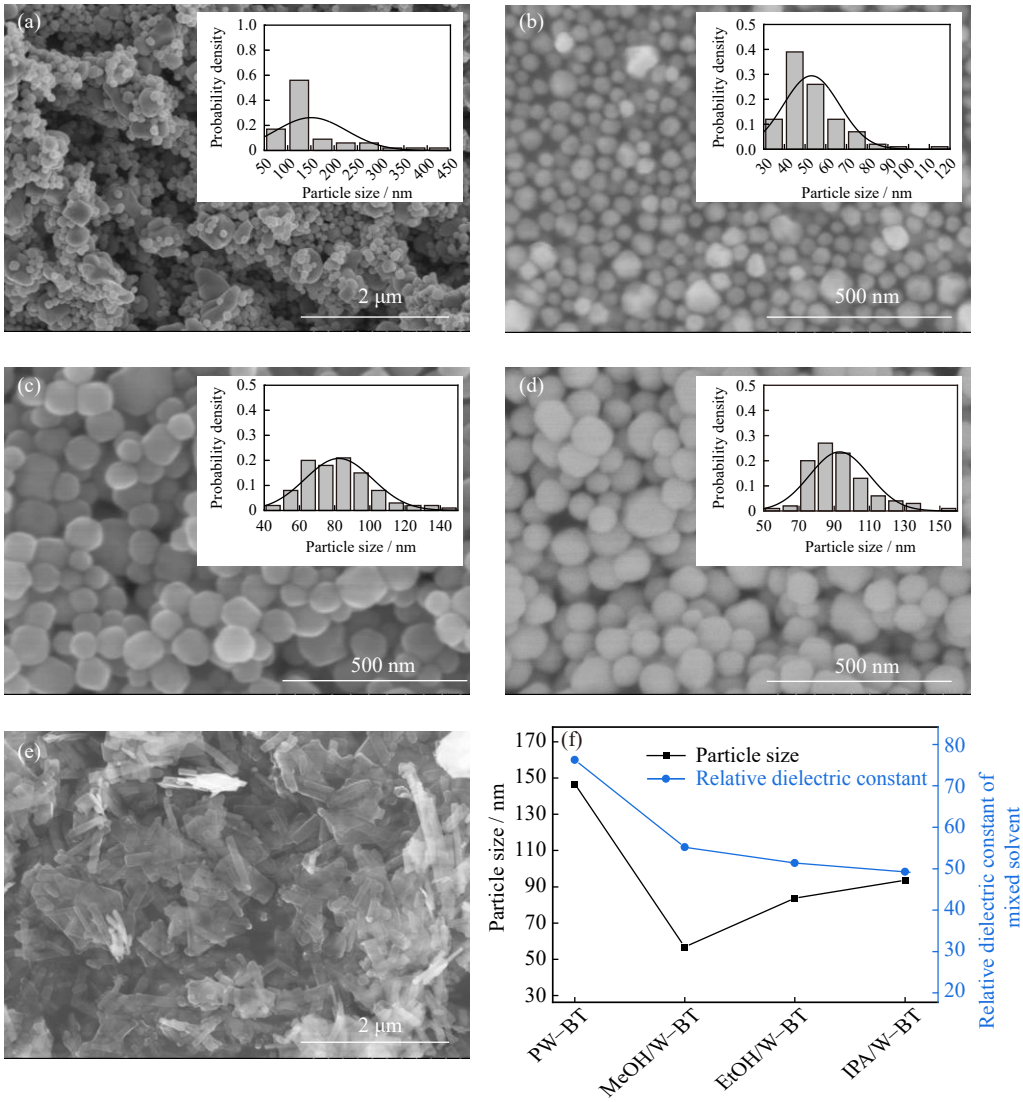

Fig. 4. SEM images of (a) PW–BT, (b) MeOH/W–BT, (c) EtOH/W–BT, (d) IPA/W–BT, and (e) EG/W–BT samples. The inset of (a)–(d) exhibits the particle size distribution of the corresponding samples based on SEM. (f) Average particle sizes of PW–BT, MeOH/W–BT, EtOH/W–BT, and IPA/W–BT samples and dielectric constant of corresponding mixed solvent.

has a large range of particle sizes. The particle size distribution is not even, mostly around the average particle size of 151 nm. The particle size of the MeOH/W–BT sample is concentrated around 40–60 nm. For EtOH/W–BT and IPA/W–BT samples, particle sizes are uniformly distributed on both sides of the mean particle sizes (82 and 93 nm, respectively) following a standard normal distribution. Among these approximately spherical $BaTiO_3$ particles, the particle size of samples synthesized in pure water is the largest (Fig. 4(f)). After the addition of monohydric alcohols to the reaction medium, the range of particle size distribution becomes narrow and decreases. The particle size decreases in the order of isopropanol, ethanol, and methanol, with the smallest particle size observed in the presence of methanol. Evidently, the particle size of $BaTiO_3$ is associated with the physicochemical properties of water and alcohols shown in Table 2. The dielectric constant (ε) is introduced to characterize the polarity of the solvent environment and investigate solvent effects [39]. The dielectric constant of the mixed solvent (ε_{mix}) is calculated in accordance with the volume proportion of alcohol and water based on the following equation [40–41]: $\varepsilon_{mix} = \varepsilon_{alcohol} \times \varphi_1 + \varepsilon_{water} \times \varphi_2$, where $\varepsilon_{alcohol}$ and ε_{water} refer to the dielectric constant of alcohol and water (Table 2), and φ_1 and φ_2 represent the volume percentages of alcohol and water, respectively. The relationship between particle size and the dielectric constant of mixed solvent is presented in Fig. 4(f). As the reaction medium changes from pure water to a mixed solution of alcohol and water, the dielectric constant decreases, accompanied by a decrease in particle size. Moreover, the particle size gradually increases as the dielectric constants of mixed solvents further decrease. Considering that the dielectric constant of alcohol is lower than that of water, the solubility of precursors in monohydric alcohol/water mixed solvents is lower than that in pure water [38]. Precursors are prone to supersaturation in monohydric alcohol/water mixed solvents, which promotes massive crystal nucleation and hinders crystal growth during the dissolution–precipitation process [25,42]. Consequently, the addition of monohydric alcohols with low dielectric constant results in a smaller particle size. In addition, the boiling point and viscosity of the solvent have a great influence on the particle size. For samples synthesized in monohydric alcohol/water mixed solvents, the average particle size decreases with the decrease of boiling point and viscosity of alcohol solvents (Table 2) and reaches a minimum value under the condition of methanol. The low boiling point and viscosity can promote the mass transference of reactive species, which further facilitates crystal nucleation [43]. Plenty of crystal nuclei formed simultaneously promote the formation of $BaTiO_3$ nanoparticles with a narrow particle size distribution [44].

Table 2. Physicochemical properties of water and alcohols

Solvent	Boiling point / °C	Viscosity / (mPa·s)	Relative dielectric constant
Water	100	1	78.5
Methanol	64.7	0.6	32.7
Ethanol	78.3	1.074	24.5
Isopropyl alcohol	82.4	2.3	19.92
Ethylene glycol	197.3	25.66	37.7

3.4. TEM analysis

TEM was performed to explore the microstructure of the samples. Fig. 5 exhibits the TEM images of $BaTiO_3$ synthesized in different solvents. The PW–BT sample has a smooth particle surface and a tetrahedral shape with rounded corners (Fig. 5(a)). The size of the particles ranges between 100 and 150 nm, which is consistent with the calculated result based on SEM (Fig. 4(a)). The $BaTiO_3$ synthesized in monohydric alcohol/water mixed solvents is approximately spherical in shape (Fig. 5(b)–(d)). The particles have a smooth surface and good dispersion. The particle sizes are uniformly distributed and consistent with the results calculated by SEM (Fig. 4(f)). The internal pores are observed in particles of PW–BT, MeOH/W–BT, and IPA/W–BT synthesized by hydrothermal method, which is a common defect in $BaTiO_3$ inevitably affecting the tetragonal characteristics [45]. The internal pores are almost circular. For the EG/W–BT sample, particles are long flakes and tend to stack together (Fig. 5(e)).

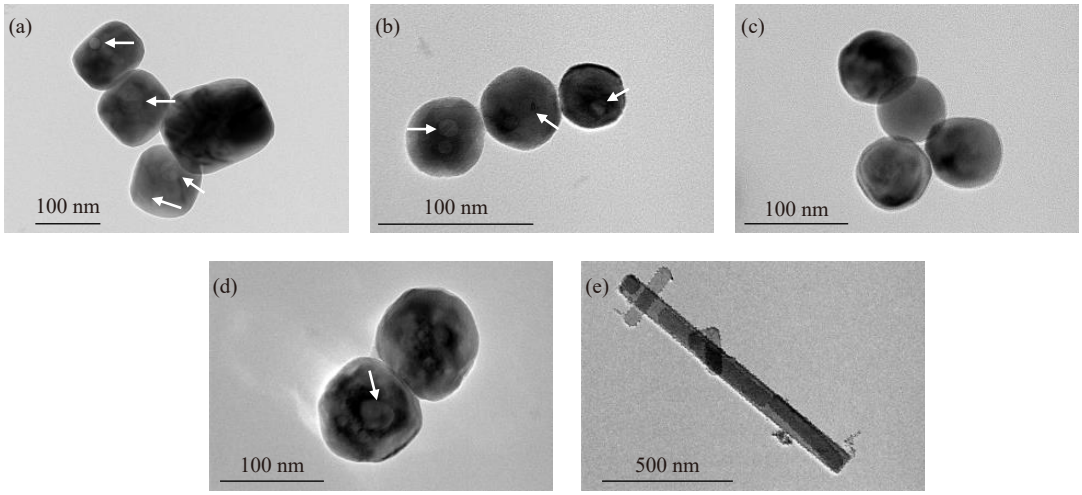

Fig. 5. TEM images of (a) PW–BT, (b) MeOH/W–BT, (c) EtOH/W–BT, (d) IPA/W–BT, and (e) EG/W–BT samples.

The lengths vary and the widths range from 50 to 80 nm. The edge around the flaky particles is similar to blunt teeth, which may be attached by tiny impurity particles.

Fig. 6 shows high-resolution transmission electron microscopy (HRTEM) images of $BaTiO_3$ samples synthesized in different solvents. The lattice fringes of Fig. 6(a)–(d) are regularly arranged, indicating that the observed particles are well crystallized. The HRTEM image of the representative EtOH/W–BT nanoparticle (Fig. 6(c)) shows that the measured lattice spacings (*d*) are 0.400 nm and 0.281 nm, which are well attributed to the (100) and (110) planes of tetragonal $BaTiO_3$. The well-developed lattice fringes for (111), (001), or (110) planes are clearly observed at particles of PW–BT, MeOH/W–BT, and IPA/W–BT, respectively. In contrast, the HRTEM of the EG/W–BT sample displays lattice fringes in multiple directions (Fig. 6(e)), revealing that particles are composed of multiple tiny and randomly orientated grains. The clear lattice fringe spacings of 0.394 nm and 0.195 nm are ascribed to the (100) and (200) crystal planes of tetragonal $BaTiO_3$.

The selected area electron diffraction (SAED) patterns of $BaTiO_3$ samples synthesized in different solvents are provided in Fig. 7. The SAED patterns in Fig. 7(a)–(d) show that the observed $BaTiO_3$ nanoparticles are all confirmed as the single crystal phase, which can be indexed as tetragonal structure. Diffraction rings of EG/W–BT in Fig. 7(e) consist of discrete diffraction spots, revealing the polycrystalline properties of the nanoparticles.

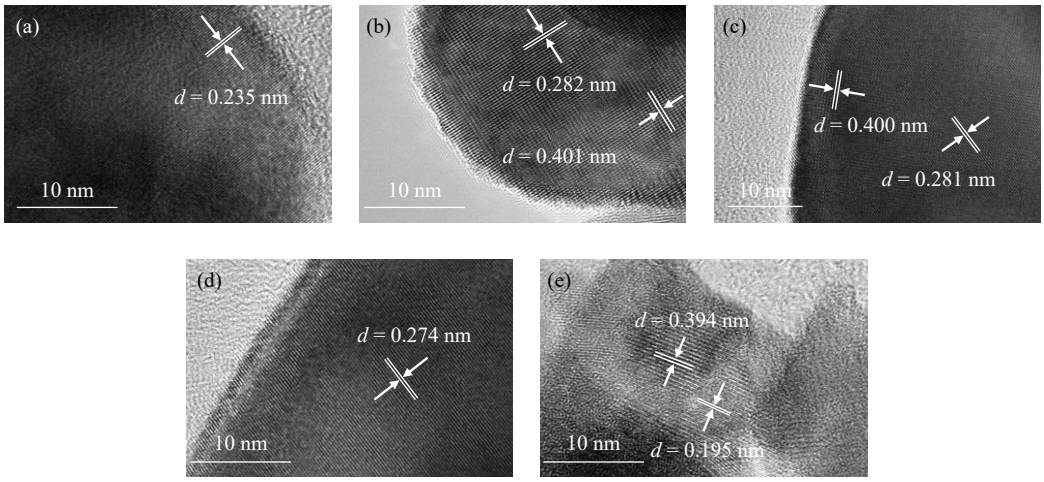

Fig. 6. HRTEM images of (a) PW–BT, (b) MeOH/W–BT, (c) EtOH/W–BT, (d) IPA/W–BT, and (e) EG/W–BT samples.

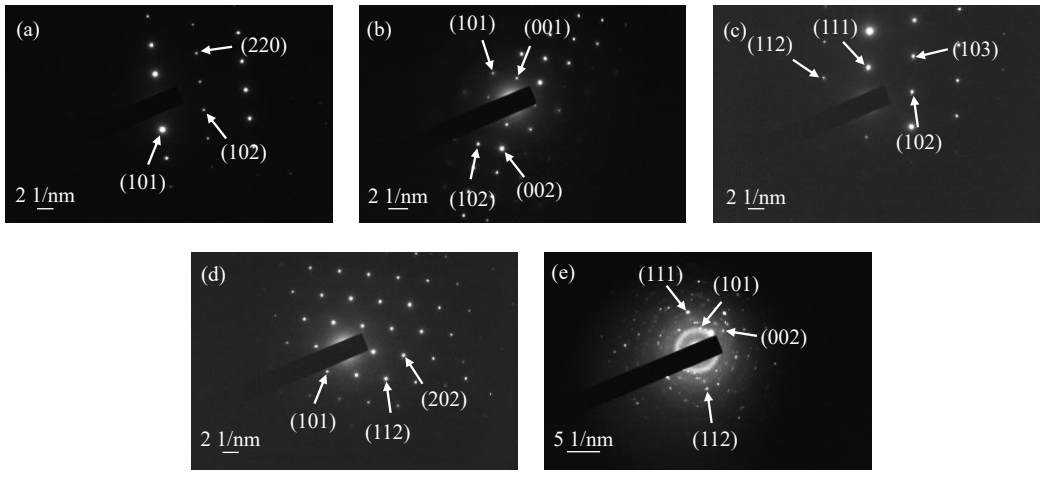

Fig. 7. SAED patterns of (a) PW–BT, (b) MeOH/W–BT, (c) EtOH/W–BT, (d) IPA/W–BT, and (e) EG/W–BT samples.

3.5. BET analysis

The specific surface area and pore size distribution of $BaTiO_3$ powders were investigated by N_2 adsorption and desorption test. As listed in Table 3, PW–BT, MeOH/W–BT, EtOH/W–BT, and IPA/W–BT samples exhibit specific surface areas of 7.23, 17.30, 11.87, and 10.67 $m^2 \cdot g^{-1}$. Fig. 8(a) manifests the typical H3 class closed hysteresis loops with downward protrusions in the whole pressure range in the Brunauer–Emmett–Teller (BET) isotherms of $BaTiO_3$ powders, indicating the porous structure [46–48]. Fig. 8(b) demonstrates the pore size distribution of PW–BT, EtOH/W–BT, and IPA/W–BT samples, which is a typical distribution of microporous and mesoporous structures. MeOH/W–BT displays a partially larger pore size, corresponding to the largest average pore diameter shown in Table 3. The smallest average pore diameter of EtOH/W–BT

Table 3. Specific surface area and pore size of the samples

Sample	SSA / ($m^2 \cdot g^{-1}$)	d_{BET} / nm	Average pore diameter / nm
PW–BT	7.23	136.49	14.66
MeOH/W–BT	17.3	57.04	28.45
EtOH/W–BT	11.87	83.14	11.43
IPA/W–BT	10.67	92.49	13.39

further illustrates that ethanol/water is the most favorable medium for the growth and development of tetragonal $BaTiO_3$ particles in the media studied.

From the above results, the solvent has a great effect on the structure, morphology, and particle size distribution of $BaTiO_3$. There is a nonlinear relationship between solvent type and tetragonal properties. When pure water is used as the hydrothermal medium, $BaTiO_3$ presents the highest tetragonality (c/a = 1.0090). This is closely followed by the tetragonality of the EtOH/W–BT sample (c/a = 1.0088). In addition to the rod-shaped particles of EG/W–BT, particles prepared in other media conditions are approximately spherical. Among them, particles synthesized in the monohydric alcohol/water media have a more uniform size distribution and better dispersion than the PW–BT sample. In the case of alcohol-containing solvents, the particle size decreases in the order of isopropanol, ethanol, and methanol. The structure and morphology of particles are related to the physicochemical properties of hydrothermal media. Among the obtained particles, the PW–BT sample has the highest tetragonality, the largest particle size and the agglomeration. The MeOH/W–BT sample has the smallest particle size and the lowest tetragonality. By comparison, the optimum condition for synthesizing $BaTiO_3$ with ethanol/water as the medium is determined. The high tetragonality (c/a = 1.0088) and small average particle size (82 nm) of the EtOH/W–BT sample meet the requirements of MLCCs for a thin dielectric layer and ultra-high capacity.

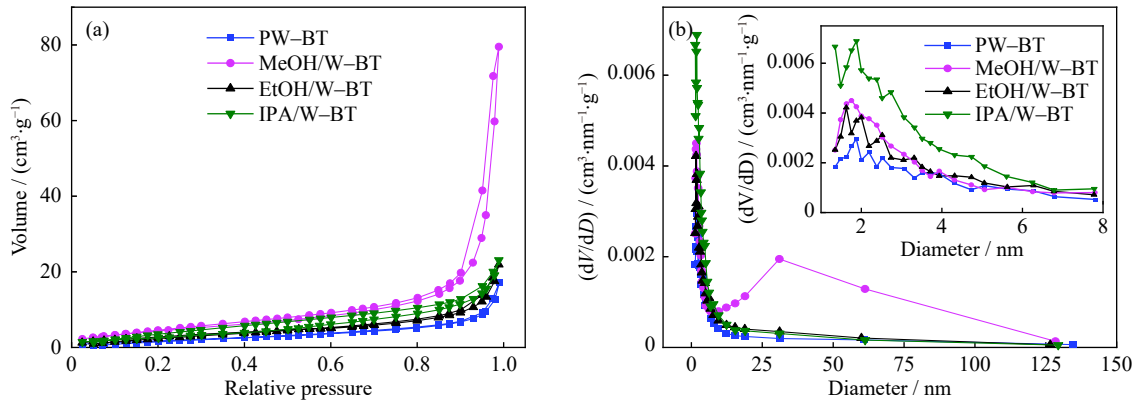

Fig. 8. (a) BET isotherms and (b) pore size distributions of PW–BT, MeOH/W–BT, EtOH/W–BT, and IPA/W–BT samples.

4. Conclusion

This study showed that tetragonal $BaTiO_3$ were synthesized by using a simple one-step hydrothermal process. The method used $Ba(OH)_2 \cdot 8H_2O$ and $TiCl_4$ as raw materials at 240°C. The solvent affects the adequacy of the hydrothermal reaction and the crystal structure. Water with the highest dielectric constants results in the highest tetragonality of $BaTiO_3$. Among the studied alcohols, the effect of ethanol in promoting the formation of the tetragonal structure is the most significant. In addition, the dielectric constant, boiling point, and viscosity of solvents have a large influence on the morphology of nanoparticles. With a decrease in dielectric constants, the average size of the particles synthesized in monohydric alcohol/water mixed solvents is smaller than that synthesized in pure water. In the case of alcohol-containing solvents, the average particle size decreases in the order of isopropanol, ethanol, and methanol with the decrease of boiling point and viscosity. Furthermore, the optimal condition for synthesizing tetragonal $BaTiO_3$ involves the use of ethanol/water as the solvent. The obtained $BaTiO_3$ maintains high tetragonality (c/a = 1.0088) and small average particle size (82 nm), leading to better properties for application in miniaturized MLCCs.

Acknowledgements

This work was supported by Chongqing Newcent New Materials Co., Ltd., China (No. 2021GKF-0708).

Conflict of Interest

The authors declare no conflicts of interest.

References

[1] I. Pasuk, F. Neațu, Ş. Neațu, *et al*., Structural details of $BaTiO_3$ nano-powders deduced from the anisotropic XRD peak broadening, *Nanomaterials*, 11(2021), No. 5, art. No. 1121.

[2] D. Mao, Z. Zhang, M. Yang, Z.M. Wang, R.B. Yu, and D. Wang, Constructing $BaTiO_3/TiO_2$@polypyrrole composites with hollow multishelled structure for enhanced electromagnetic wave absorbing properties, *Int. J. Miner. Metall. Mater.*, 30(2023), No. 3, p. 581.

[3] L. Wang, J.Q. Lv, F. Shi, K.X. Song, W. Lei, H.F. Zhou, Z.M. Qi, and J. Wang, Intrinsic dielectric properties and lattice vibrational characteristics of single phase $BaTiO_3$ ceramic, *J. Mater. Sci.: Mater. Electron.*, 32(2021), No. 19, p. 24041.

[4] Y. Liu, S.F. Wang, Z.J. Chen, and L.X. Xiao, Applications of ferroelectrics in photovoltaic devices, *Sci. China Mater.*, 59(2016), No. 10, p. 851.
[5] G. Bolla, H.L. Dong, Y.G. Zhen, Z.H. Wang, and W.P. Hu, Organic cocrystals: The development of ferroelectric properties, *Sci. China Mater.*, 59(2016), No. 7, p. 523.
[6] L. Lv, Y. Wang, L. Gan, Q. Liu, and J.P. Zhou, Sintering process effect on the $BaTiO_3$ ceramic properties with the hydrothermally prepared powders, *J. Mater. Sci.: Mater. Electron.*, 29(2018), No. 17, p. 14883.
[7] E. Song, D.H. Kim, E.J. Jeong, *et al*., Effects of particle size and polymorph type of TiO_2 on the properties of $BaTiO_3$ nanopowder prepared by solid-state reaction, *Environ. Res.*, 202(2021), art. No. 111668.
[8] K. Suzuki and K. Kijima, Phase transformation of $BaTiO_3$ nanoparticles synthesized by RF-plasma CVD, *J. Alloys Compd.*, 419(2006), No. 1-2, p. 234.
[9] R.J. Li, W.X. Wei, J.L. Hai, L.X. Gao, Z.W. Gao, and Y.Y. Fan, Preparation and electric-field response of novel tetragonal barium titanate, *J. Alloys Compd.*, 574(2013), p. 212.
[10] O. Kucuk, S. Teber, I.C. Kaya, H. Akyildiz, and V. Kalem, Photocatalytic activity and dielectric properties of hydrothermally derived tetragonal $BaTiO_3$ nanoparticles using TiO_2 nanofibers, *J. Alloys Compd.*, 765(2018), p. 82.
[11] J.M. Han, M.R. Joung, J.S. Kim, *et al*., Hydrothermal synthesis of $BaTiO_3$ nanopowders using TiO_2 nanoparticles, *J. Am. Ceram. Soc.*, 97(2014), No. 2, p. 346.
[12] Y. Shi, Y.P. Pu, Y.F. Cui, and Y.J. Luo, Enhanced grain size effect on electrical characteristics of fine-grained $BaTiO_3$ ceramics, *J. Mater. Sci.: Mater. Electron.*, 28(2017), No. 17, p. 13229.
[13] T.T. Lee, C.Y. Huang, C.Y. Chang, *et al*., Phase evolution of solid-state $BaTiO_3$ powder prepared with the ultrafine $BaCO_3$ and TiO_2, *J. Mater. Res.*, 27(2012), No. 19, p. 2495.
[14] J.L. Clabel H, I.T. Awan, A.H. Pinto, *et al*., Insights on the mechanism of solid state reaction between TiO_2 and $BaCO_3$ to produce $BaTiO_3$ powders: The role of calcination, milling, and mixing solvent, *Ceram. Int.*, 46(2020), No. 3, p. 2987.
[15] A.A. Kholodkova, M.N. Danchevskaya, Y.D. Ivakin, *et al*., Solid state synthesis of barium titanate in air and in supercritical water: Properties of powder and ceramics, *Ceram. Int.*, 45(2019), No. 17, p. 23050.
[16] S. Wang, Y. Zhang, Z. Ji, Y.S. Gu, Y.H. Huang, and C. Zhou, Characterization and growth dynamics of barium titanate crystallite on nanometer scale, *J. Univ. Sci. Technol. Beijing* (*Engl. Ed.*), 12(2005), No. 1, p. 33.
[17] R.A. Surmenev, R.V. Chernozem, A.G. Skirtach, *et al*., Hydrothermal synthesis of barium titanate nano/microrods and particle agglomerates using a sodium titanate precursor, *Ceram. Int.*, 47(2021), No. 7, p. 8904.
[18] M. Li, L.L. Gu, T. Li, *et al*., TiO_2-seeded hydrothermal growth of spherical $BaTiO_3$ nanocrystals for capacitor energy-storage application, *Crystals*, 10(2020), No. 3, art. No. 202.
[19] Y.F. Peng, H.L. Chen, F. Shi, and J. Wang, Effect of polyethylene glycol on $BaTiO_3$ nanoparticles prepared by hydrothermal preparation, *IET Nanodielectr.*, 3(2020), No. 3, p. 69.
[20] H. Hayashi and T. Ebina, Effect of hydrothermal temperature on the tetragonality of $BaTiO_3$ nanoparticles and *in-situ* Raman spectroscopy under tetragonal–cubic transformation, *J. Ceram. Soc. Jpn.*, 126(2018), No. 3, p. 214.
[21] J.B. Gao, H.Y. Shi, H.N. Dong, R. Zhang, and D.L. Chen, Factors influencing formation of highly dispersed $BaTiO_3$ nanospheres with uniform sizes in static hydrothermal synthesis, *J Nanopart Res*, 17(2015), No. 7, art. No. 286.
[22] İ.C. Kaya, V. Kalem, and H. Akyildiz, Hydrothermal synthesis of pseudocubic $BaTiO_3$ nanoparticles using TiO_2 nanofibers: Study on photocatalytic and dielectric properties, *Int. J. Appl. Ceram. Technol.*, 16(2019), No. 4, p. 1557.
[23] Y.A. Huang, B. Lu, D.D. Li, *et al*., Control of tetragonality via dehydroxylation of $BaTiO_3$ ultrafine powders, *Ceram. Int.*, 43(2017), No. 18, p. 16462.
[24] N.N. Hasbullah, S.K. Chen, K.B. Tan, Z.A. Talib, J.Y.C. Liew, and O.J. Lee, Photoluminescence activity of $BaTiO_3$ nanocubes via facile hydrothermal synthesis, *J. Mater. Sci.: Mater. Electron.*, 30(2019), No. 5, p. 5149.
[25] S. Yin and T. Hasegawa, Morphology control of transition metal oxides by liquid-phase process and their material development, *KONA Powder Part. J.*, 40(2023), p. 94.
[26] X.K. Mo, Y.F. Liu, and Y.J. Li, Effect of additives on particle characteristics of barium titanate nanopowder by hydrothermal synthesis, *Mater. Res. Innov.*, 12(2008), No. 1, p. 35.
[27] K. Nakashima, K. Onagi, Y. Kobayashi, *et al*., Stabilization of size-controlled $BaTiO_3$ nanocubes via precise solvothermal crystal growth and their anomalous surface compositional reconstruction, *ACS Omega*, 6(2021), No. 14, p. 9410.
[28] H.Q. Qi, L. Fang, W.T. Xie, H.Q. Zhou, Y. Wang, and C. Peng, Study on the hydrothermal synthesis of barium titanate nanopowders and calcination parameters, *J. Mater. Sci.: Mater. Electron.*, 26(2015), No. 11, p. 8555.
[29] M.M. Wu, J.B. Long, G.G. Wang, *et al*., Hydrothermal synthesis of tetragonal barium titanate from barium hydroxide and titanium dioxide under moderate conditions, *J. Am. Ceram. Soc.*, 82(1999), No. 11, p. 3254.
[30] C.Y. Su, Y. Otsuka, C.Y. Huang, *et al*., Grain growth and crystallinity of ultrafine barium titanate particles prepared by various routes, *Ceram. Int.*, 39(2013), No. 6, p. 6673.
[31] C. Baek, J.H. Yun, H.S. Wang, *et al*., Enhanced output performance of a lead-free nanocomposite generator using $BaTiO_3$ nanoparticles and nanowires filler, *Appl. Surf. Sci.*, 429(2018), p. 164.
[32] J. Adam, G. Klein, and T. Lehnert, Hydroxyl content of $BaTiO_3$ nanoparticles with varied size, *J. Am. Ceram. Soc.*, 96(2013), No. 9, p. 2987.
[33] H.W. Lee, S. Moon, C.H. Choi, and D.K. Kim, Synthesis and size control of tetragonal barium titanate nanopowders by facile solvothermal method, *J. Am. Ceram. Soc.*, 95(2012), No. 8, p. 2429.
[34] D.V. On, L.D. Vuong, T.V. Chuong, D.A. Quang, H.V. Tuyen, and V.T. Tung, Influence of sintering behavior on the microstructure and electrical properties of $BaTiO_3$ lead-free ceramics from hydrothermal synthesized precursor nanoparticles, *J. Adv. Dielectr.*, 11(2021), No. 2, art. No. 2150014.
[35] M. Maček Kržmanc, D. Klement, B. Jančar, and D. Suvorov, Hydrothermal conditions for the formation of tetragonal $BaTiO_3$ particles from potassium titanate and barium salt, *Ceram. Int.*, 41(2015), No. 10, p. 15128.
[36] M. Özen, M. Mertens, F. Snijkers, and P. Cool, Hydrothermal synthesis and formation mechanism of tetragonal barium titanate in a highly concentrated alkaline solution, *Ceram. Int.*, 42(2016), No. 9, p. 10967.
[37] Z.F. Zhang, W.B. Wang, and A.Q. Wang, Effects of solvothermal process on the physicochemical and adsorption characteristics of palygorskite, *Appl. Clay Sci.*, 107(2015), p. 230.
[38] M. Inada, N. Enomoto, K. Hayashi, J. Hojo, and S. Komarneni, Facile synthesis of nanorods of tetragonal barium titanate using ethylene glycol, *Ceram. Int.*, 41(2015), No. 4, p. 5581.
[39] A.D. Han, X.H. Yan, J.R. Chen, X.J. Cheng, and J.L. Zhang, Effects of dispersion solvents on proton conduction behavior of ultrathin Nafion films in the catalyst layers of proton exchange membrane fuel cells, *Acta Phys. Chim. Sin.*, 38(2022), No. 3, art. No. 1912052.
[40] Y.H. Xu, D. Zheng, W.X. Ji, N. Abu-Zahra, and D.Y. Qu, A molecular dynamics study of the binding effectiveness between undoped conjugated polymer binders and tetra-sulfides in lithi-

um–sulfur batteries, *Composite Part B*, 206(2021), art. No. 108531.

[41] W.E. Moore, The use of an approximate dielectric constant to blend solvent systems, *J. Am. Pharm. Assoc. Sci. Ed.*, 47(1958), No. 12, p. 855.

[42] Y.J. Yan, H. Xia, Y.Q. Fu, Z.Z. Xu, and Q.Q. Ni, Controlled hydrothermal synthesis of different sizes of $BaTiO_3$ nanoparticles for microwave absorption, *Mater. Res. Express*, 6(2020), No. 12, art. No. 1250i3.

[43] R.Y. Guo, Y. Bao, Q.L. Kang, C. Liu, W.B. Zhang, and Q. Zhu, Solvent-controlled synthesis and photocatalytic activity of hollow TiO_2 microspheres prepared by the solvothermal method, *Colloids Surf. A*, 633(2022), art. No. 127931.

[44] K. Nakashima, K. Hironaka, K. Oouchi, *et al*., Optimizing TiO_2 through water-soluble Ti complexes as raw material for controlling particle size and distribution of synthesized $BaTiO_3$ nanocubes, *ACS Omega*, 6(2021), No. 48, p. 32517.

[45] C. Baek, J.E. Wang, S. Moon, C.H. Choi, and D.K. Kim, Formation and accumulation of intragranular pores in the hydrothermally synthesized barium titanate nanoparticles, *J. Am. Ceram. Soc.*, 99(2016), No. 11, p. 3802.

[46] K.X. Wang, S. Wang, K.S. Hui, *et al*., Synergistically boosting the elementary reactions over multiheterogeneous ordered macroporous Mo_2C/NC–Ru for highly efficient alkaline hydrogen evolution, *Carbon Energy*, 4(2022), No. 5, p. 856.

[47] Z. Su, H.Y. Ling, M. Li, *et al*., Honeycomb-like carbon materials derived from coffee extract via a “salty” thermal treatment for high-performance Li–I_2 batteries, *Carbon Energy*, 2(2020), No. 2, p. 265.

[48] Z.N. Lei, X.Y. Ma, X.Y. Hu, J. Fan, and E.Z. Liu, Enhancement of photocatalytic H_2-evolution kinetics through the dual cocatalyst activity of Ni_2P–NiS-decorated g-C_3N_4 heterojunctions, *Acta Phys. Chim. Sin.*, 38(2022), No. 7, art. No. 2110049.